MODELING THE CRYSTALLIZATION OF MARTIAN IGNEOUS COMPOSITIONS. J. Semprich[1] and J. Filiberto[2], [1]AstrobiologyOU, The Open University, Walton Hall, Milton Keynes, MK7 6AA, UK (julia.semprich@open.ac.uk), [2]ARES Division, XI3, NASA Johnson Space Center, Houston, TX 77058, USA

Introduction: The martian crust is dominated by basalts and ultramafic rocks [1]. Understanding the crystallization sequence of martian igneous rocks is critical for constraining the petrologic and geochemical evolution of the crust and mantle. Experimental studies have investigated the parental liquid compositions and crystallization behavior using martian meteorite compositions [2-7], as well as compositions measured by rovers on the martian surface [8,9]. While experiments deliver crucial results, they are often limited by time and resources. Therefore, modeling approaches are an ideal tool to complement experimental results.

The application of the MELTS software package [10, 11], to calculate the crystallization of martian compositions, reproduces important compositional details of magma crystallization but significant uncertainties regarding the pressure of the olivine-pyroxene multiple saturation point have been reported [12], and in the temperatures of initial crystallization [12, 13]. Recently, a new melting model, MAGMARS, has been shown to reproduce martian primary melts more accurately [14].

Here, we constrain the applicability of Gibbs free energy minimization software Perple_X [15] for martian compositions by comparing our modeled results to experimentally derived crystallization paths for two martian compositions.

Methods: We model phase equilibria for a bulk composition resembling the Zagami meteorite [3] and an experimental glass composition [8] based on Humphrey, an Adirondack basalt in Gusev crater [16, 17]. Due to the low water content reported in the martian interior [18, 19], we use anhydrous compositions. MnO, P_2O_5, NiO, and Cr_2O_3 are not included in our calculations. We use the Gibbs free energy minimization program Perple_X [15] version 6.8.7 in combination with the hp633ver.dat data base [20]. Solid solution models for melt, clinopyroxene, olivine, and spinel are taken from [21]. For plagioclase, we use the $I\bar{1}$ model [22]. To model the crystallization sequence at 1 bar for Zagami, two setups are used for different oxidation states: 1) all FeO is assumed to be divalent; and 2) O_2 is set as an unconstrained saturated component and the fayalite-magnetite-quartz (FMQ) buffer is selected in the thermodynamic data file. To model phase stabilities at higher pressure for Humphrey, we set O_2 as

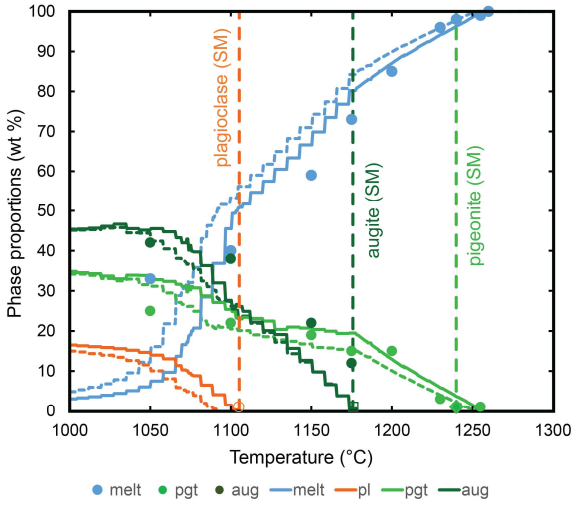

Figure 1. Comparison of experimental and modeled crystallization temperatures for the composition of Zagami (in wt.%): 51.3 SiO_2, 0.81 TiO_2, 6.18 Al_2O_3, 17.8 FeO, 10.3 MgO, 10.6 CaO, 1.29 Na_2O, 0.13 K_2O. Phases shown are pigeonite (light green), augite (dark green), plagioclase (orange), and melt (blue). Circles: mineral proportions (wt.%) from experiments [3]. Dashed vertical lines represent crystallization temperatures from [2]. Solid lines: model results with divalent iron; dashed lines: model results using the FMQ buffer.

unconstrained saturated component and calculate with the FMQ and the quartz-iron-fayalite (QIF) buffers.

Results: Fig. 1 shows a comparison of our modeled results with those obtained by equilibrium experimental studies of the Zagami composition at 1 bar [2, 3]. The experimental liquidus is between 1255-1260 °C [3], and at 1240 °C [2]. The modeled liquidus is at 1257 °C (FeO) and at 1250 °C (FMQ) and therefore either within the range of experimental data or ± 10 °C. The composition of pigeonite at liquidus temperatures in experimental studies is $Fs_{21}Wo_5$ [3] and $Fs_{22}Wo_7$ [2]. Modeled pigeonite compositions are with $Fs_{20.5}Wo_{3.9}$ (FeO) and $Fs_{18.2}Wo_{3.9}$ (FMQ) relatively close although slightly more magnesian than the experimental compositions. The first augite crystallizes at 1175 and 1176 °C in experiments [2, 3] and at similar temperatures of 1178 °C in the model for both conditions. Experimental augite compositions at these temperatures are between $Fs_{19.9}Wo_{30.2}$ [3] and $Fs_{15.6}Wo_{37}$ [2]. The modeled augite compositions are with $Fs_{17.7}Wo_{33.1}$ (FeO) and $Fs_{15.6}Wo_{34.6}$ (FMQ) within this range. However, experiments and models differ in

the amount of augite: experiments report an estimated 12 wt. % augite [3], whereas the model starts with traces although the amount of augite increases rapidly upon cooling. Feldspar crystallization was not observed in experiments by [3] but was reported to occur within the temperature range of 1182-1105 °C by [2]. In our models, plagioclase crystallizes at 1104 °C (FeO) and at 1091 °C (FMQ) and is therefore within the range of experimental results.

A comparison of experimental [8] and modeled results for the Humphrey composition is shown in Fig. 2. Experimental results estimate the multiple saturation point with both olivine and pigeonite on the liquidus at approximately 12.5 kbar and 1375 °C [8]. The modeled multiple saturation point in calculations with FMQ buffer is approximately at 11.9 kbar and 1375 °C and therefore at slightly lower pressure at the same temperature. The modeled pigeonite composition at these conditions is $Fs_{19.8}Wo_{2.8}$, which is somewhat more magnesian and less calcian than the experimental pigeonite $Fs_{24}Wo_{11}$ observed at 1350 °C and 11.7 kbar [8]. In the model with the QIF buffer, the multiple saturation point is estimated to be at ~ 14.3 kbar and ~1394 °C and therefore at higher temperatures and pressures than conditions obtained from experiments. The corresponding pigeonite composition at these conditions is $Fs_{22.1}Wo_{3.2}$.

Discussion and conclusions: Models presented here have been calculated without the addition of Cr_2O_3, which is expected to influence the stability of Cr-spinel and the effect of Cr on phase diagrams will have to be evaluated in future models. The other excluded oxides (MnO, P_2O_5, NiO) are only present in small amounts in the starting compositions and are therefore not expected to significantly change the modeled crystallization temperatures and estimates of the multiple saturation points.

Models at 1 bar using the starting composition of Zagami predict the crystallization temperatures of pigeonite, augite, and plagioclase within ± 10 °C of experiments with mineral compositions relatively close to the ones observed but show some differences in mineral modes. Model calculations at higher pressures using the composition of Humphrey, at the FMQ buffer, results in a multiple saturation point at the same temperature and within 0.6 kbar compared to experimental estimates. Calculations with the QIF buffer result in at multiple saturation point ~ 20 °C and ~ 1.8 kbar higher than in experiments.

While additional martian compositions and the influence of certain oxides still need further testing with this approach, we conclude that Perple_X models of martian crystallization temperatures and multi

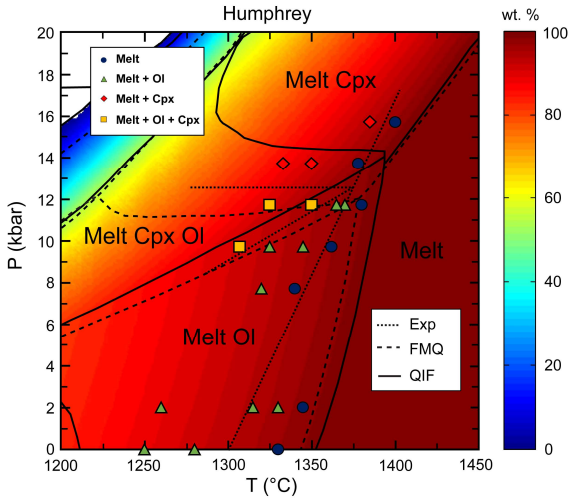

Figure 2. Comparison of experimental and modeled phase fields for the composition of Humphrey (in wt.%): 45.99 SiO_2, 0.56 TiO_2, 10.89 Al_2O_3, 20.01 FeO, 10.89 MgO, 8.12 CaO, 2.44 Na_2O, 0.1 K_2O. Symbols and the dotted line represent experimental results [8]. The dashed line represents model results set to the FMQ buffer, and solid black lines were obtained for the QIF buffer. The color scale illustrates the amount of melt in the composition (in wt. %).

saturation point conditions produce robust results when directly compared to experiments.

References: [1] McSween H.Y. (2015) *AmMin, 100*, 2380–2395. [2] Stolper E.M. and McSween H.Y. (1979) *GCA, 43,* 1475-1498. [3] McCoy T.J. and Lofgren G.E. (1999) *EPSL, 173,* 397-411. [4] Musselwhite D.S. et al. (2006) *MAPS, 41*, 1271-1290. [5] Filiberto J. (2008) *GCA, 72*, 690-701. [6] Filiberto J. et al. (2010) *MAPS, 45*, 1258-1270. [7] Filiberto J. and Dasgupta R. (2011) *EPSL, 304*, 527-537. [8] Filiberto J. et al. (2008) *MAPS, 43*, 1137-1146. [9] Filiberto J. et al. (2010) *GRL, 37*, L13201. [10] Ghiorso M.S and Sack R.O. (1995) *ContribMinPet, 119*, 197-212. [11] Ghiorso M.S. et al. (2002), *G^3, 3*, 1-35. [12] Balta J.B. and McSween H.Y.(2013) *JGR, 118*, 2502-2519. [13] Gross, J. et al. (2013) *MAPS, 48*, 854-871. [14] Collinet, M. et al. (2021) *JGR, 126*, e2021JJE006985. [15] Connolly J. A. D. (2005) *EPSL, 236*, 524-541. [16] Gellert R. et al (2006) *JGR, 111*, E02S05. [17] McSween H.Y. et al. (2006) *JGR, 111,* E0S10. [18] Filiberto J. et al. (2016) *MAPS, 51*, 2023-2035. [19] McCubbin F.M. et al. (2016) *MAPS, 51*, 2036-2060. [20] Holland T.J.B. and Powell R. (2011) *J Metamorph Geol, 29*, 333-383. [21] Holland T.J.B et al. (2018*) J Pet, 59*, 881-900. [22] Holland T.J.B. and Powell R. (2003) *Contrib Min Pet, 145*, 492-501.